

Structure, Conductivity, and Ionic Motion in $\text{Na}_{1+x}\text{Zr}_2\text{Si}_x\text{P}_{3-x}\text{O}_{12}$: A Simulation Study

P. Padma Kumar[†] and S. Yashonath*

Solid State and Structural Chemistry Unit, Indian Institute of Science, Bangalore, India - 560 012

Received: January 30, 2002; In Final Form: April 30, 2002

Constant-pressure, constant-temperature variable-shape simulation cell Monte Carlo and microcanonical ensemble molecular dynamics simulation of superionic conducting rhombohedral phase of Nasicon, $\text{Na}_{1+x}\text{Zr}_2\text{Si}_x\text{P}_{3-x}\text{O}_{12}$, $0 \leq x \leq 3$, at a temperature of 600 K is reported. Changes in structure, conductivity, hop path, site occupancies, bond lengths of framework atoms with composition are discussed. Average Na(1)–O distance shows a peak at $x = 2$, while Na(2)–O distance shows a monotonic increase. Sum of the sodium occupancies at Na(1) and mid-Na sites adds up to a constant value of one which supports the conclusion of Boilot et al.¹ based on X-ray diffraction. Occupancy of Na(1) site attains a minimum at $x = 2$. The predominant conduction channel (which carries more than 90% of the sodium ions) is found to be the one connecting Na(1)–mid-Na–Na(2). Density contours for sodium, depicting this conduction channel, are reported. Free energy profile along the conduction channel suggests that entropy contribution cannot be neglected. The mid-Na site is not associated with a free energy minimum.

I. Introduction

The discovery of $\text{NaZr}_2(\text{PO}_4)_3$ by Hong² and Goodenough et al.³ attracted considerable attention of materials scientists. In his pioneering work Hong showed that it is possible to synthesize a series of materials of the general formula $\text{Na}_{1+x}\text{Zr}_2\text{Si}_x\text{P}_{3-x}\text{O}_{12}$ with $0 \leq x \leq 3$ and that the material $\text{Na}_3\text{Zr}_2\text{Si}_2\text{PO}_{12}$ (the composition with $x = 2$) is an excellent ionic conductor. The conductivity of $\text{Na}_3\text{Zr}_2\text{Si}_2\text{PO}_{12}$ above 443 K was found to be comparable to that of Na- β -alumina, with many an advantage in practical applications as a fast ion conductor.² Henceforth, materials with topology and structure similar to those of $\text{Na}_3\text{Zr}_2\text{Si}_2\text{PO}_{12}$ are referred to as Nasicons (for Na-SuperIonic Conductors), irrespective of whether they classify as superionic conductors or not and whether other alkali ions replace Na. Apart from being potential candidates as solid electrolytes, Nasicon-type materials find enormous applications in nuclear waste disposal,⁴ as gas sensors, as low expansion ceramics,^{4–6} and as thermal-shock-resistant materials.⁷ Recently the porous glasses of Nasicons have been found to show promising catalytic activities as well.⁸

These materials exhibit many useful as well as interesting properties which are often attributed to their unique structural features. They have an open framework structure, consisting of corner-linked ZrO_6 -octahedra and $(\text{Si/P})\text{O}_4$ -tetrahedra. The resulting covalently bonded framework is highly stable and at the same time flexible. This flexibility allows it to incorporate alkali ions of different sizes (Li^+ , Na^+ , K^+ , Rb^+ , and Cs^+) and for certain alkali ions such as Na^+ , in varying amounts as well.^{2,6} These materials in general exhibit low and anisotropic thermal expansions. It is also possible to synthesize near zero-thermal expansion materials of Nasicons, through incorporation of suitable ions such as Ca and Sr in the alkali ion sites⁴ or by replacing a few of the tetravalent ions (Zr ions) by Na ions.⁵

The low-temperature structure of $\text{Na}_{1+x}\text{Zr}_2\text{Si}_x\text{P}_{3-x}\text{O}_{12}$ for $x < 1.6$ and $x > 2.4$ is rhombohedral (hexagonal) with an $\text{R}\bar{3}\text{c}$

space group.^{2,9} The compounds in the above range of compositions are not known to exhibit any phase transitions up to their melting points ($> 1650^\circ\text{C}$). At low temperature, the members of $\text{Na}_{1+x}\text{Zr}_2\text{Si}_x\text{P}_{3-x}\text{O}_{12}$ in the range $1.6 < x < 2.4$ (the SICs) show a slight distortion to the monoclinic structure and the space group is $\text{B}2/\text{c}$.^{1,2,9,10} This low-temperature monoclinic structure transforms to rhombohedral structure at around $T_1 \approx 420\text{ K}$.^{1,9} This transition is suggested to be a second-order λ transition. The transition is also accompanied by an increase in conductivity and over the transition region ($400\text{ K} < T_1 < 460\text{ K}$) the activation energy gradually reduces to half its value in the monoclinic phase.^{9,10}

The high-temperature rhombohedral $\text{R}\bar{3}\text{c}$ -phase is the one of particular interest here, due to its high ionic conductivity. A particularly interesting aspect of $\text{Na}_{1+x}\text{Zr}_2\text{Si}_x\text{P}_{3-x}\text{O}_{12}$ is that as the composition, x , increases the conductivity initially increases, by many orders of magnitude, up to an $x \approx 2$. Beyond this it decreases showing⁹ an anomalous peak near $x = 2$. This anomalous variation in conductivity with composition is associated with a similar anomalous variation of the c -axis of the rhombohedral unit cell.¹ Many authors have attributed the high conductivity around $x = 2$, to the opening up of the bottleneck caused by the peak in the c -axis near $x = 2$.^{11,12} In contrast, Boilot et al.,¹ who have carried out a comprehensive study of anomalous variation in conductivity, conclude that the most important single reason for the high Na^+ conductivity observed near $x = 2$ is the high sodium–sodium correlation arising from their strong Coulombic repulsion.¹ More careful investigations are needed to obtain insight into which of these two factors plays a major role in the observed increase in conductivity. Different groups have suggested different pathways for Na^+ migration.^{11,13,14} Even after numerous experimental investigations, in the past three decades, many aspects of the ionic motion in these materials remain poorly understood.

Recently a few theoretical efforts have also been made to understand some of these aspects of ionic motion in Nasicon-type solids. Martinez-Juárez et al.¹⁵ have studied the effect of the size of the bottleneck on Li^+ motion in $\text{LiMM}(\text{PO}_4)_3$, where

* Corresponding author. E-mail: yashonath@sscu.iisc.ernet.in.

[†] E-mail: padma@sscu.iisc.ernet.in.

M, M' = Ge, Ti, Sn, Hf. They employ a Distance Least Square (DLS) method to substantiate their experimental findings. Yet another interesting study in the present context is by Daniele Mazza,¹⁶ who has investigated the variation in activation energy with composition as well as the preferred ionic pathway for conduction. An interesting observation of the study is that distortion of the structure, from the ideally stacked polyhedra, enhances the conductivity. The study makes use of a bond valence equation (BVE) and suffers from some limitations as it is based on a rigid framework model—neglecting the framework motions—and long-range Coulombic interactions are not accounted for.¹⁶ These methods also have the inherent drawback of not being able to probe ion dynamics.

Classical molecular dynamics (MD) and Monte Carlo (MC) techniques have been extensively used, as complementary to experimental probes, in elucidating the nature of the ionic motion and related aspects of superionic conductors in the last three decades. These simulation techniques make use of a model interionic potential that can reproduce the well-established experimental results. Of the most successful model potentials in the past, those by Vashishta and Rahman on AgI¹⁷ and by Walker and Catlow on Na- β -alumina¹⁸ are particularly noteworthy. The development of interionic potentials are quite tedious, particularly in the case of relatively complex materials such as Nasicons. Recently we have proposed a model potential¹⁹ to study Li⁺ motion in LiZr₂(PO₄)₃ that correctly reproduces the known properties of these solids. The model was subsequently employed to understand the dependence of ion mobility in Nasicon-type solids on the size of the mobile ion as well as the size of the bottleneck.²⁰ In these MD simulations using the proposed¹⁹ model interionic pair potential, the framework was kept rigid and only the variables associated with Li⁺ ions were integrated. This model would be found inadequate in the study of Na_{1+x}Zr₂Si_xP_{3-x}O₁₂, where considerable distortions of the framework (through coupled rotations of the polyhedra) and variation in lattice parameters are observed with composition x .^{1,21} Recently, we have proposed a complete interionic potential between alkali ion and other atoms of the framework as well as between the framework atoms themselves.²² This potential seems to predict the variation of lattice parameters and conductivity on composition correctly.²² Here we report extensive simulations at eight different compositions ($x = 0, 0.5, 1.0, 1.5, 2.0, 2.5, 2.7$, and 3.0). Analysis of MD trajectories is carried out to derive insight into structure, conductivity, ion occupancy at various sites, hop path from one site to another, and free energy. These provide fresh insights into ion conduction in these materials.

II. Intermolecular Potential

An interionic pair potential proposed recently,²²

$$\phi(r_{ij}) = \frac{q_i q_j r_{ij}}{r_{ij}} + \frac{A_{ij}(\sigma_i + \sigma_j)^{n_{ij}}}{r_{ij}^{n_{ij}}} - \frac{C_{ij}}{r_{ij}^6} \quad (1)$$

where q_i is the charge and σ_i is the ionic radii of the i th ion, has been employed in the present study. A_{ij} and C_{ij} are, respectively, the overlap-repulsive energy and dispersion energy of ion pairs i and j . Here i and j refer to Na, Zr, Si, P, and O.

The parameters of the potential have been determined by fitting to the structure and conductivity of just one single composition ($x = 2$), viz., Na₃Zr₂Si₂PO₁₂, at just one single temperature, $T \sim 600$ K in the following way.

An account of the strategy adopted in deriving the parameters of the interionic potential for Na_{1+x}Zr₂Si_xP_{3-x}O₁₂:

TABLE 1: Interaction Potential Parameters for X–O (where X = Na, Zr, Si, P, and O)^a

species X	q_X ($ e $)	σ_X (Å)	A_{XO} (eV)	C_{XO} (eV Å ⁶)	n_{XO}
Na	0.702	1.13	0.1716	0.000	9
Zr	2.808	0.86	1.2126	11.917	9
Si	2.808	0.40	2.8059	11.529	9
P	3.510	0.31	3.6158	9.279	9
O	−1.404	1.21	0.3252	47.999	7

^a $A_{Na Na} = 5$ eV, $n_{Na Na} = 11$, and all the other A_{ij} and C_{ij} values that are not listed above are assumed to be zero.

1. A set of initial values were chosen to start with for the parameters q_i , A_{ij} , and C_{ij} . The values of σ were taken from Huheey.²³

2. The A_{ij} and C_{ij} values were adjusted to reproduce the bond lengths, coordination numbers of bonded species, and rdf's (obtained from MD simulations at 600 K) of the experimental X-ray structure²⁴ at $x = 2$ and 623 K.

3. The pressures again obtained from MD simulations were adjusted to yield as close a value as possible to the atmospheric pressure by adjusting the charges and C_{ij} values.

4. The former were more effective in obtaining the correct pressure. We also ensured that the melting point of the solid is high by suitable scaling of all parameters.

5. A_{NaO} is adjusted to reproduce the conductivity.

6. Parameters associated with Na–Na interaction also influence the properties.

MD is carried out iteratively after every refined set of parameters. Every time, the resulting structure and conductivity from MD are compared with experiments and further adjustments in parameters are made based on the criteria discussed above. The procedure is repeated until MD results are close to the experimental data. It may be noted that a change in a single parameter can alter several properties and adjustment in more than one parameter is required to get agreement in a single property. The above-discussed procedure is one of the many ways of achieving an optimized set of parameters. The parameters are given in Table 1.

III. Simulation Details

We have chosen to carry out constant-temperature and constant-pressure Monte Carlo calculations with variable-shape simulation cell²⁵ (NPT-MC) to obtain the lattice parameters. Microcanonical ensemble molecular dynamics (NVE-MD) simulations²⁶ have been carried out to obtain structural and dynamical properties. The lattice parameters for the latter simulation were those obtained from NPT-MC simulations. This procedure was adopted for the following reason. First, dynamical properties of interest are best obtained from MD simulations performed in the microcanonical ensemble rather than canonical or NPT ensemble since the latter requires a somewhat arbitrary choice of W_s , the mass associated with the s variable in the Nose formulation.²⁷ There is no unambiguous way of choosing W_s . This procedure will yield results identical to those obtained from constant-pressure, constant-temperature MD simulations.

A. NPT-MC Simulation. Variable-shape NPT-MC simulations at 600 K and 1 atm pressure were carried out initially. The starting configuration for these runs were the X-ray diffraction structure of Boilot et al.²⁴ Note that X-ray studies are unable to distinguish between the Si and P positions. Their positions were therefore fixed such that they are evenly distributed in the Si/P site across the unit cell at the beginning of the simulation. Displacements to alter the size and shape of the simulation cell are attempted every four MC moves. Each

MC move consists of an attempt to move all the particles within the simulation cell once, chosen sequentially. Properties are calculated for 20×10^3 MC steps after devoting 15×10^3 steps for proper equilibration of the system. These simulations yield the volume and cell parameters (a , b , c , α , β , and γ) as well as the atomic positions under a given set of external conditions. Simulations have been carried out for eight different compositions, $x = 0, 0.5, 1.0, 1.5, 2, 2.5, 2.7$, and 3 . Size of the simulated system is $3 \times 3 \times 1$ unit cells. At $x = 0$, $N = 972$ ions which progressively increases to 1134 for $x = 3$. The simulation cell is of size $26.673 \times 26.673 \times 22.87$ Å at $x = 0$. A cut-off radius of 11.4 Å has been employed.

B. NVE-MD Simulation. The NVE-MD simulations were performed, at the desired temperature of 600 K, in a rhombohedral simulation cell with cell parameters (a , b , and c) obtained from variable-shape NPT-MC simulations. The initial configuration of ions for the NVE-MD simulations were the final configurations from NPT-MC simulations. Initial velocities were chosen from a Maxwellian velocity distribution for 600 K. The velocity form of the Verlet algorithm with an integration time step $\Delta t = 2.5$ fs is found to yield good energy conservation. An equilibration of over 200 ps was followed by a production run of 1 ns. For four compositions ($x = 0, 1, 2$, and 3) NVE-MD simulations were carried out with lattice parameters at $T \sim 600$ K reported by X-ray^{5,14,24} and neutron¹² diffraction studies as well. The results are essentially the same.

IV. Results and Discussion

A. Framework Structure. The structure (R $\bar{3}c$) of Nasicons may be described as consisting of corner-sharing PO₄/SiO₄ tetrahedra and ZrO₆ octahedra interconnected to give rise to a three-dimensional network through which the alkali ions can move. Each octahedron is connected to six tetrahedra and each tetrahedron is connected to four octahedra. Zr–O, Si–O, and P–O radial distribution functions (rdf's) are shown in Figure 1(a–c) for the low-temperature structure, R $\bar{3}c$, at $x = 0, 1, 2$, and 3 . For comparison, we indicate the position of the peak for the $x = 2$ composition of Nasicon reported by Boilot et al.²⁴ using X-ray diffraction, by means of vertical lines, (height of the line proportional to the intensity). The average bond lengths for bonded pairs (Zr–O, Si–O, and P–O) have been obtained by averaging over all first coordination oxygen shells of the corresponding atom and over all MD steps. These are compared with the X-ray^{14,24,28} and neutron¹² diffraction values in Table 2. Changes in the bond lengths of Zr–O, Si–O and P–O with composition may be seen. The coordination numbers for Zr, Si and P are seen to be 6, 4 and 4 oxygens at all compositions as expected. In addition, average Na(1)–O, Na(2)–O and mid Na–O distances are listed in Table 2. These have been obtained when the Na⁺ is within 0.8 Å of the corresponding site (Na(1), Na(2), or mid-Na).

Bond angles in Nasicons may play an important role in the changes observed in both structure and conductivity with composition. Table 3 lists the average O–Zr–O, O–Si–O, O–P–O, Zr–O–Si, and Zr–O–P bond angles at different compositions along with X-ray diffraction results reported by Hazen et al.²⁸ for $x = 0.11$. The O–Zr–O, O–Si–O, and O–P–O are the angles within the polyhedra and are expected to be more stiff, while Zr–O–Si and Zr–O–P are the angles between polyhedra whose flexibility is important for rotation of polyhedra which have been found to play an important role in structural and other property variations with composition. Note that the O–Zr–O and O–(Si/P)–O angles are close to 90° and 109.5°, respectively, suggesting the presence of ideal

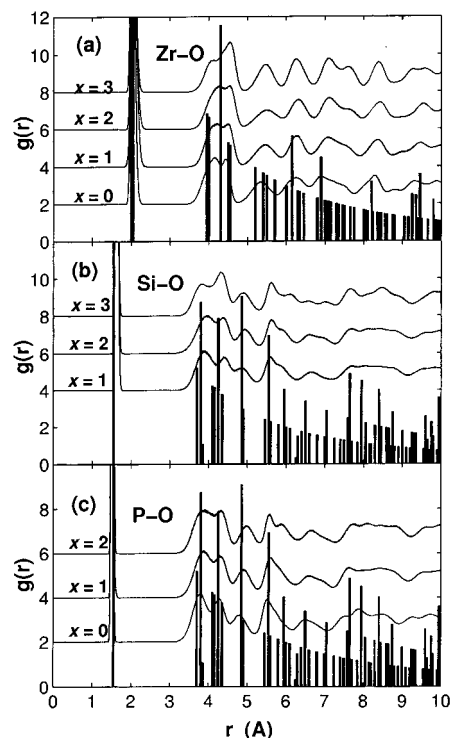


Figure 1. The radial distribution functions (rdf's) for ion pairs (a) Zr–O, (b) Si–O, and (c) P–O for four compositions ($x = 0, 1, 2$, and 3), from NVE-MD at 600 K, are compared with those from the experimental structure of Na₃Zr₂Si₂PO₁₂. The rdf's from NVE-MD are displaced along the Y-axis for clarity. The rdf's calculated from the X-ray structure²⁴ is shown as a bar plot.

TABLE 2: The Na–O Distances at Na(1), Na(2), and Mid-Na Sites as Well as the Zr–O, Si–O, and P–O Bond Lengths from NVE-MD Are Compared with Experiments

x	Na(1)–O Å	Na(2)–O Å	(mid-Na)–O Å	Zr–O Å	Si–O Å	P–O Å	ref
0	2.725		2.615	2.052		1.518	
0.11	2.597			2.070		1.522	expt ²⁸
1	2.773	2.712	2.595	2.070	1.628	1.521	
1	2.657	2.671		2.072	1.552 ^a		expt ¹²
2	2.846	2.769	2.632	2.068	1.627	1.521	
2	2.703	2.686		2.074	1.588 ^a		expt ¹²
2.09	2.688	2.686	2.48	2.076	1.592 ^a		expt ²⁴
3	2.671	2.748	2.593	2.060	1.627		
3	2.540	2.709		2.084	1.622		expt ¹⁴

^a Average of Si–O and P–O bond lengths.

TABLE 3: Some Select Bond Angles (in degrees) from NVE-MD

x	O–Zr–O	O–Si–O	O–P–O	Zr–O–Si	Zr–O–P
0	89.87		109.28		155.35
0.11 ^a	89.95		109.65		150.75
1	90.06	109.04	109.25	150.44	156.18
2	89.97	109.23	109.04	152.61	156.00
3	89.92	109.26		151.68	

^a From X-ray diffraction.²⁸

octahedra and tetrahedra. The Zr–O–P angles are generally found to be larger than Zr–O–Si by about 3–5°.

It is well-known in the literature that the substitution of the larger Si ion in place of P ions and associated incorporation of counterions (Na⁺), as x increases from 0 to 3, gives rise to an anomalous increase in the c parameter of the rhombohedral cell while the a parameter increases monotonically.¹ It is interesting

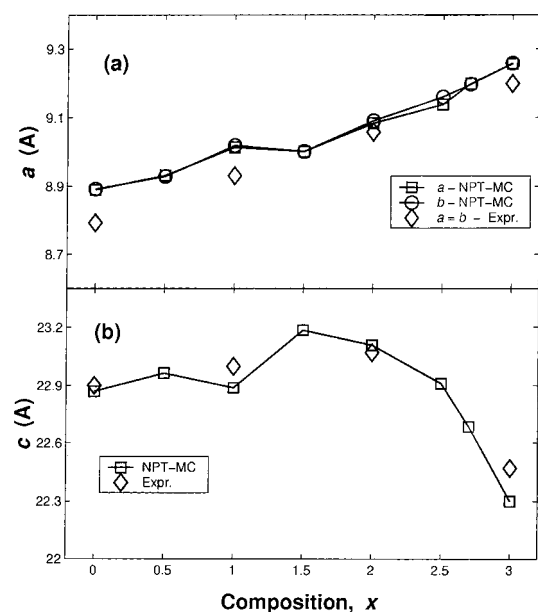


Figure 2. Variation of lattice parameters, (a) a and (b) c , as a function of x for $\text{Na}_{1+x}\text{Zr}_2\text{Si}_3\text{P}_{3-x}\text{O}_{12}$ from variable-size variable-shape NPT-MC simulation at 600 K. The a and c from NPT-MC are compared with those from X-ray diffraction performed either at 573 or at 623 K.

that the composition where the maximum of the c parameter is observed coincides with the maximum in the conductivity in these materials. Figure 2 shows the variation of the a and c parameters (obtained as a function of x from the NPT-MC simulations). It is seen that the anomalous maximum, near $x = 2$, of the c parameter (Figure 2b) as well as the monotonic increase of the a parameter (Figure 2a) are correctly reproduced by the interionic potential. The other lattice parameters, α , β , and γ (the angles of the rhombohedral unit cell), are found to be within 0.5° of the expected values, $\alpha = \beta = 90^\circ$ and $\gamma = 120^\circ$. At low compositions ($x = 0$ and 1), it is seen that the value of the lattice parameter a obtained from NPT-MC is slightly higher than the experimental value. The difference is small (≤ 0.1 Å). The difference is probably due to the limited duration of these runs, as we shall see in the next section. More detailed variation of a and c with x obtained in this study suggests that the lattice parameters are successfully reproduced over the whole composition range $0 \leq x \leq 3$. In the case of $\text{MZr}_2(\text{PO}_4)_3$, where M is Li^+ , Na^+ , K^+ , Rb^+ , or Cs^+ , the variations of the lattice parameter upon the substitution of bigger M-cations in place of Li^+ has been well studied in terms of coupled rotations of polyhedra.^{28–30} No such explanation for the variation of lattice parameters with composition has been proposed.

Overall it is seen that the geometry of the polyhedra (octahedra and tetrahedra) as well as the angles between the polyhedral units are reproduced well. The lattice parameters and their variation with composition are also in agreement with the X-ray diffraction results available in the literature suggesting that the potential is able to successfully reproduce the structure. We will now look at the other properties.

B. Conductivity and Ionic Motion. One of the most interesting and technologically important aspect of Nasicons is their high ionic conductivity. As already explained, the ionic conductivity of these materials exhibit an anomalous peak near $x = 2$ when plotted as a function of composition.^{1,9} This compound at $x = 2$ has a conductivity of $\sigma = 0.35 \Omega^{-1} \text{cm}^{-1}$ at 573 K which is comparable to that of the β -alumina ($\text{Na}_2\text{O} \cdot x\text{Al}_2\text{O}_3$).^{1,2} The Nasicons have certain important advantages,

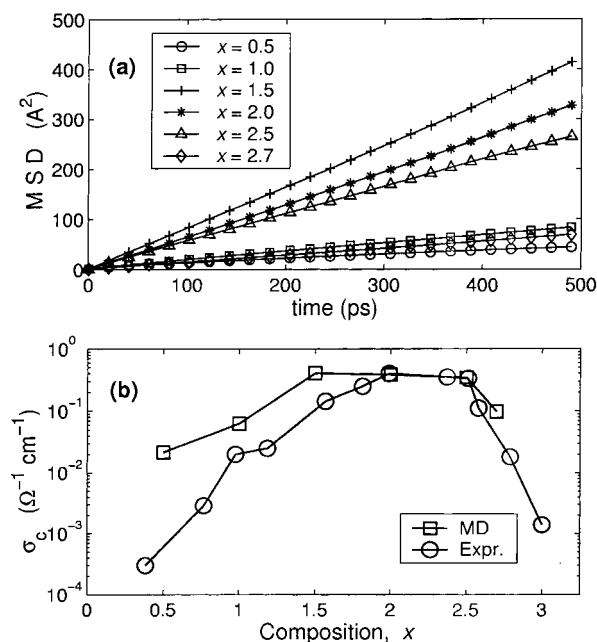


Figure 3. (a) MSDs, from NVE-MD, for different compositions, x , and (b) conductivity, σ_c , as a function of x , for $\text{Na}_{1+x}\text{Zr}_2\text{Si}_3\text{P}_{3-x}\text{O}_{12}$ from NVE-MD is shown.

such as near isotropic (three-dimensional) mobility of ions, easier synthetic routes, lower sintering temperature, low thermal expansivities, etc., over β -alumina. These are important advantages particularly when considering these materials for battery applications.

The phosphate end member ($x = 0$) of $\text{Na}_{1+x}\text{Zr}_2\text{Si}_3\text{P}_{3-x}\text{O}_{12}$ is a poor conductor¹ (conductivity, $\sigma_c \approx 2.5 \times 10^{-5} \Omega^{-1} \text{cm}^{-1}$ at $T = 573$ K) as is the case with the silicate end member¹⁴ (with $x = 3$, $\sigma_c = 3.5 \times 10^{-4} \Omega^{-1} \text{cm}^{-1}$ at 573 K). As we go up the series with increasing Na^+ content the conductivity rises quite sharply, reaches a maximum ($\sigma_c = 3.5 \times 10^{-1} \Omega^{-1} \text{cm}^{-1}$, at $T = 573$ K) when $x \approx 2$ and then falls off¹ even more sharply when x approaches 3. The members of the series with composition in the range of $1.6 < x < 2.4$ have high conductivities above 573 K and therefore qualifies as a superionic conductor. Figure 3a shows the evolution of mean square displacement (MSD) of Na^+ ions with time for compositions $x = 0.5, 1.0, 1.5, 2.0, 2.5$, and 2.7 . For the two end members (not shown), $x = 0$ and $x = 3$, the MSD reaches a plateau within 2 ps at 0.52 and 0.44 Å^2 , respectively. The diffusion coefficient (D) of the Na^+ ions for each of these compositions is calculated from the slope of the respective MSD. The conductivity, σ_c , is calculated using the Nernst–Einstein relation,

$$\sigma_c = \frac{N_{\text{Na}} e^2 D}{V k_B T} \quad (2)$$

where N_{Na} is the number of Na^+ ions in the simulation cell of volume V , D is the diffusivity at temperature T , and k_B is the Boltzmann's constant. The conductivity calculated from the above expression for the various compositions is plotted in Figure 3b. Also shown are the experimental values from Boilot et al.¹ It may be seen that the variation of σ_c with x including the anomalous maximum near $x = 2$ is correctly reproduced. For the two end members $x = 0$ and 3, the diffusion coefficient and hence the conductivity is too low and MD is unable to estimate the values correctly. Alternative ways, such as those suggested by Chandler and co-workers,^{31,32} may need to be employed at these compositions. At $x = 0.5, 1$, and 2.7 , where

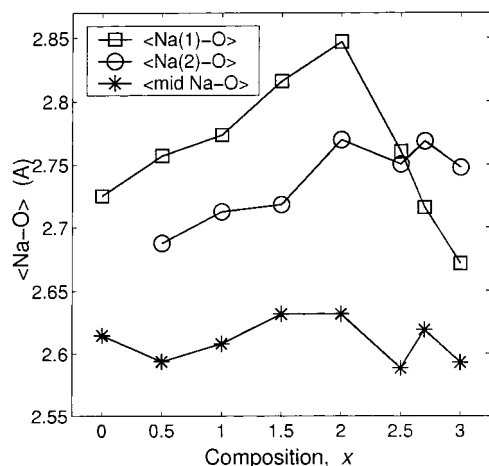


Figure 4. The variation of Na–O distances for Na(1) (Na(1)–O), Na(2) (Na(2)–O), and mid-Na ((mid-Na)–O) sites as a function of composition, x , obtained from NVE-MD simulations.

the conductivity is still not very high, MD results are higher than reported by experiments. The difference is again attributable to the slow relaxation. This aspect is evident from the MSD which shows a deviation from linearity. Further, the reduced slope toward the tail (400–500 ps) suggests that longer runs might yield lower values of diffusion coefficients and provide more accurate estimates.

1. Na⁺ Occupancies. It is well-known that framework structures with a large number of partially occupied sites with good connectivity across them (pathways with low energetic barriers connecting them) are good candidates for superionic conductor. The Nasicon-framework, [Zr₂((Si/P)O₄)₃], is one which offers a large number of sites for Na⁺ to occupy. In the case of rhombohedral Na_{1+x}Zr₂Si_xP_{3-x}O₁₂, several authors have identified that there are prominently two crystallographically distinct sites Na(1) (the 6b positions) and Na(2) (the 18e positions) which the Na⁺ ions can occupy.^{2,11–14,33} Cherkaoui et al. in their NMR investigation on NaZr₂(PO₄)₃ have suggested that apart from these two sites a third site (referred to as mid-Na site) of low occupancy exists in the pathway connecting the Na(1) and Na(2) sites and midway between the two.³⁴ Later single-crystal X-ray diffraction experiments on Na₃Zr₂Si₂PO₁₂ by Boilot et al. found that there is considerable Na⁺ occupancy in the mid-Na site (36f positions), particularly near $x = 2$ composition.^{1,24}

The maximum in the conductivity coincides with the maximum in the c parameter.¹ To understand the relationship between these, we looked at the changes in the framework with composition, x . The Na(1) site is at the center of a distorted oxygen octahedra (Na(1)O₆) which is sandwiched between two ZrO₆ along the c axis. The Na(2) site, on the other hand, is irregularly eight-coordinated with oxygens forming a Na(2)O₈ polyhedra which is located between the ribbons forming the framework. The mid-Na site is five-coordinated with oxygen (forming mid-NaO₅ polyhedra), out of the five oxygens three are part of the Na(1)O₆ while the other two belong to the Na(2)O₈. Figure 4 shows the variation of the Na–O distance at the three sites (denoted as, Na(1)–O, Na(2)–O, and (mid-Na)–O) as a function of composition x . The Na–O distance at the various sites also serves as a good measure of the sizes of the corresponding Na–O polyhedra. It is seen that the Na(1)O₆ increases initially, as x increases, shows a maximum around $x = 2$ and then falls off anomalously when $x = 3$. The Na(2)O₈ shows a slight expansion as x increases. These observations are in good qualitative agreement with the X-ray diffraction results

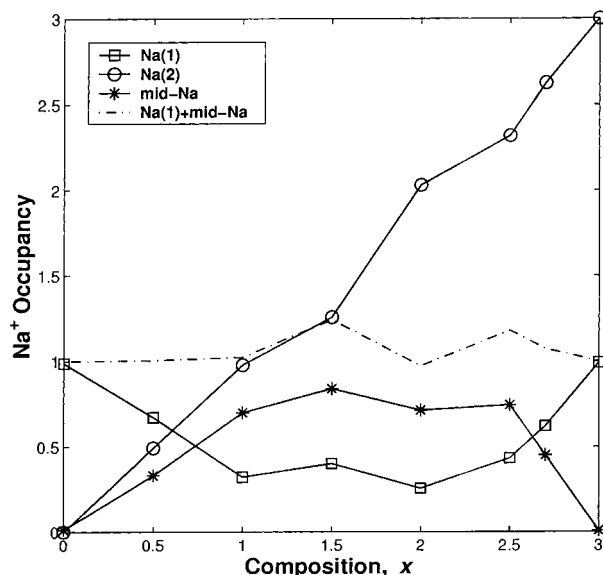
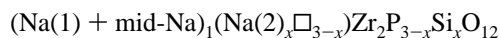


Figure 5. The occupancies of Na⁺, given as the number of Na⁺ ions per unit formula (1 + x), in the various sites (Na(1), Na(2), and mid-Na), obtained from NVE-MD simulations. The sum of the occupancies in Na(1) and mid-Na is also shown.

at 443 K by Boilot et al.¹ The (mid-Na)–O appears to be more or less constant (within the error bars of simulation) over the whole range of compositions. Considering the fact that the Na(1)O₆ lies between two rigid ZrO₆ along the c axis the anomalous expansion of the Na(1)O₆ with x seems to be associated with a similar change in the c axis. The slight expansion of the Na(2)O₈ with x is probably related to the a parameter expansion.

Figure 5 shows the Na⁺ occupancy as a function of composition from NVE-MD at 600 K. It is found that as x increases from 0 the occupancy of Na(1) decreases initially, from one, until it reaches a minimum at $x = 2$ and then increases to its original value of one when $x = 3$. On the contrary the occupancy of the mid-Na site shows an anomalous maximum, again, around $x = 2$. Here we assign a Na⁺ ion to a given site if that ion is within a distance of 0.8 Å from the site position. The position of Na(1), Na(2), and mid-Na were taken from X-ray studies at $x = 2.0$ composition by Boilot et al.²⁴ With composition the site positions alter slightly and therefore this may not be the best definition. However, it provides an idea of how site occupancies vary with composition. It appears that the anomalous increase in the mid-Na occupancy is at the expense of Na(1) occupancy since the sum of the two (broken line) appears to maintain a constant of one, over the entire range of composition. The occupancy of the Na(2) site is found to be monotonically increasing with x from a value of zero at $x = 0$ to the maximum possible value of 3 at $x = 3$. Boilot et al. have examined this aspect of site occupancies and their possible relevance to the conductivity of Na_{1+x}Zr₂Si_xP_{3-x}O₁₂.¹ They have suggested a chemical formula:



This equation describes that at all compositions the Na(1) and mid-Na sites share one Na⁺ (per unit formula), while the excess, $x\text{Na}^+$, occupies Na(2) leaving the rest $(3 - x)\text{Na(2)}$ sites vacant. The simulation results are in remarkable agreement with this view of Boilot et al.¹

Figure 6 shows the Na⁺–Na⁺ rdf's for four different compositions ($x = 0, 1, 2$, and 3). The Na⁺–Na⁺ rdf's at $x =$

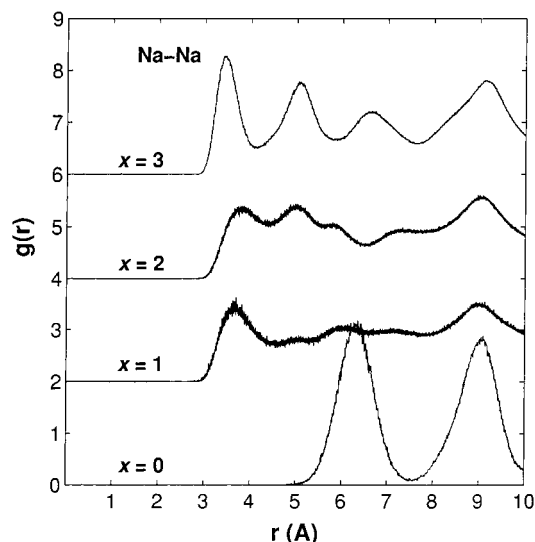


Figure 6. The $\text{Na}^+\text{--Na}^+$ rdf for four compositions, $x = 0, 1, 2$, and 3 , for $\text{Na}_{1+x}\text{Zr}_2\text{Si}_x\text{P}_{3-x}\text{O}_{12}$, from NVE-MD simulations. The sharp peaks seen for the $x = 0$ and $x = 3$ compositions suggest the localization of Na^+ ions while the broad diffuse peaks for $x = 1$ and $x = 2$ suggest the highly delocalized, long-range motion of ions.

0 shows two peaks at ~ 6.3 and 9.1 Å. These distances correspond to first and second nearest neighbor distances of Na(1) (the 6b position) with respect to another Na(1) site. Hence this indicates that for $x = 0$ the Na^+ ions are localized in Na(1) positions. For $x = 1$ and 2 , more peaks appear in the $\text{Na}^+\text{--Na}^+$ rdf's indicating that the Na^+ ions are now distributed over other available sites (the Na(2) and the mid-Na sites) as well. The peaks are diffuse which indicate that Na^+ are delocalized. This results in a higher degree of spatial disorder of the Na^+ ions. In the case of $x = 3$, the $\text{Na}^+\text{--Na}^+$ rdf shows mainly four peaks over the 10 Å distance. These peaks occur at $\approx 3.3, 4.6, 6.3$, and 9.1 Å which corresponds to the nearest neighbor Na(1) $\text{--Na}(2)$, Na(2) $\text{--Na}(2)$, Na(1) $\text{--Na}(1)$ and next nearest neighbor Na(1) $\text{--Na}(1)$ distances, respectively. This is suggestive of the fact that the Na^+ ions now fill all of Na(1) and Na(2) sites (very small occupancy may still be there at mid-Na sites). The appearance of sharper peaks for $x = 3$ (than for $x = 1$ or 2) indicates localization of Na^+ ions. The typical separation between the mid-Na site and Na(1)/Na(2) is $1.7\text{--}1.8$ Å (the exact position of the mid-Na site is found to depend on the composition). It may be noticed that the $\text{Na}^+\text{--Na}^+$ rdf does not show any peak within 2 Å in any of the compositions shown. This indicates that when a mid-Na site is occupied the nearest Na(1) and Na(2) sites are forbidden, due to high Coulombic repulsion between the Na^+ ions. The rdf's are consistent with the occupancies of Na^+ ions in the various sites shown in Figure 5.

2. Na^+ Hop Path. It is necessary to understand the exact pathway or hop path of Na^+ ions to obtain insight into the nature of ionic motion and the factors that influence ionic motion. The pathway of Na^+ ions has been the subject of much discussion in many of the earlier investigations on Nasicon. However there has been little or no convergence of ideas about this aspect. There are two possible hop paths from which Na^+ ions can choose, the Na(1) $\text{--Na}(2)$ and the Na(2) $\text{--Na}(2)$. Tran Qui et al.¹⁴ analyzing the size of the bottlenecks for ionic motion along these two paths concluded that Na(2) $\text{--Na}(2)$ hops are more probable than Na(1) $\text{--Na}(2)$ hops as the bottleneck for the Na(2) $\text{--Na}(2)$ was found to be wider (and possibly offers a lower barrier). In contrast, Kohler and Shulz^{11,13} analyzing the density distribution of Na^+ along the two paths suggested Na(1) $\text{--Na}(2)$

TABLE 4: The Fraction of the Na(1) $\text{--Na}(2)$ and Na(2) $\text{--Na}(2)$ Hops with Respect to the Total Number of Na^+ Hops at the Various Compositions, Calculated from NVE-MD^a

x	Na(1) $\text{--Na}(2)$	Na(2) $\text{--Na}(2)$
0.0	0.000	0.000
0.5	0.967	0.033
1.0	0.944	0.056
1.5	0.985	0.015
2.0	0.945	0.055
2.5	0.989	0.011
2.7	0.998	0.002
3.0	0.000	0.000

^a The Na(1) $\text{--Na}(1)$ hops were essentially zero at all values of x .

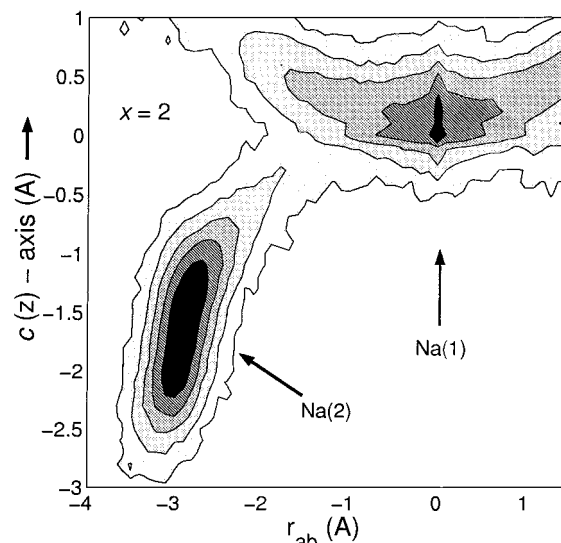


Figure 7. The density of Na^+ for $x = 2.0$ in a plane defined by the c axis and \bar{r}_{ab} which is the component, along the ab plane, of the vector joining a given Na(1) site to one of its neighboring Na(2) sites (see the text for details). An Na(1) site is chosen as the origin.

hops are more probable than Na(2) $\text{--Na}(2)$ hops. Mazza,¹⁶ on the basis of bond valence equations also suggested that it is Na(1) $\text{--Na}(2)$ hops that are more probable. The other possible hop path (Na(1) $\text{--Na}(1)$) has not been observed. In the present study we have analyzed all the possible Na^+ hops to obtain the number of Na(1) $\text{--Na}(1)$, Na(1) $\text{--Na}(2)$, and Na(2) $\text{--Na}(2)$ hops, and the results are given in Table 4. It may be seen that the majority (more than 90%) of hops are between Na(1) and Na(2), for all the compositions where Na^+ mobility is observed. The considerable occupancy of the mid-Na site provides additional evidence in support of this since the mid-Na site is located in the Na(1) $\text{--Na}(2)$ hop path. The Li^+ ion in $\text{LiZr}_2(\text{PO}_4)_3$ was also found to predominantly traverse the Na(1) $\text{--Na}(2)$ hop path, as recent MD simulations suggest.¹⁹

Figure 7 shows a contour diagram of the Na^+ in-plane density defined by the plane consisting of the c axis and the component of the vector $\bar{r}_{ab} = \bar{r} - \bar{r}_c$, where \bar{r} is the vector joining a given Na(2) with one of its neighboring but a particular Na(1) and \bar{r}_c is its component along the c axis. The density has been obtained by counting all Na^+ within a thickness of 0.05 Å of this plane over the entire run length of the NVE-MD. The contour diagram in Figure 7 appears similar to those given by Kohler and Shulz^{11,13} in their X-ray diffraction studies (see Figure 5 of ref 11 and Figure 4 of ref 13). The path is curved. It is evident from Figure 7 that Na(1) thermal ellipsoid is elongated along the ab plane and contracted along the c axis. On the contrary the Na(2) thermal ellipsoid is much longer along the c axis while shorter on the ab plane. This is in good qualitative agreement

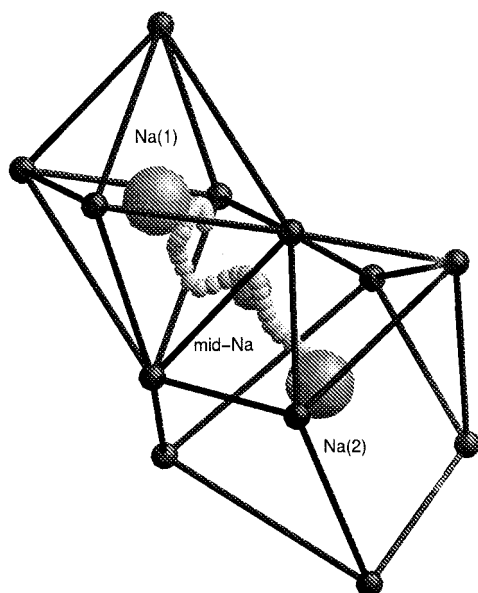


Figure 8. An MD trajectory of Na⁺ ion during a hop from Na(1) to Na(2) site. The trajectory generated corresponds to 600 K and $x = 2$ composition. The positions of Na(1), Na(2), and mid-Na sites suggested by X-ray diffraction study of Boilot et al.²⁴ is also shown as spheres.

with X-ray diffraction results of Tran Qui et al.¹⁴ and others.^{1,24} The mid-Na site is expected to appear in this conduction channel, at roughly midway, between Na(1) and Na(2) sites. But in this region no island corresponding to a local maximum in density is seen in the contour plot. Instead, a rather smooth density distribution between Na(1) and Na(2) sites is evident. Below we discuss the variation in potential energy and free energy along the hop path.

The actual trajectory of the hop from Na(1) to Na(2) is rather complex. Figure 8 shows an MD trajectory of Na⁺ ion traversing from the Na(1) to Na(2) site. This is taken from a run at 600 K and $x = 2.0$. Note that this is not the average trajectory but is one of the hop trajectories. A simplification of this trajectory in terms of a single scalar quantity indicating the progress of the hop from Na(1) to Na(2) site will be helpful in understanding the nature of potential energy and other changes along the trajectory.

Therefore, the potential energy profile of the Na⁺ ions as they execute hops from Na(1) to Na(2) (or vice versa) is calculated as a function of the distance (d_{12}) of the Na⁺ from Na(1) site. d_{12} is the distance of Na⁺ ion from Na(1) site projected along the line connecting the Na(1) to Na(2) site to which it hops. This is done by taking the dot product of the vector connecting the Na⁺ ion to Na(1) site with the Na(1)–Na(2) line. The potential energy of the Na⁺ ion is computed from

$$u_{\text{Na},i}(\vec{r}_i) = \sum_{j \neq i}^N \phi(|\vec{r}_j - \vec{r}_i|) \quad (3)$$

where N is the total number of atoms in the simulation cell and $\phi(\vec{r}_j - \vec{r}_i) \equiv \phi(r_{ij})$ is given in eq 1. The position vector of the Na(1) site from which this ion is hopping is then subtracted from \vec{r}_i and the dot product with the vector from Na(1) to Na(2) is taken to get d_{12} as mentioned above and $u_{\text{Na},i}(d_{12})$ is obtained from $u_{\text{Na},i}(\vec{r}_i)$. The potential energy profiles for three compositions, $x = 0.5$, 2, and 2.7 are shown in Figure 9. Note that the curve in Figure 9 has been obtained by averaging over the MD trajectories and include framework relaxations. The $x = 0.5$ and

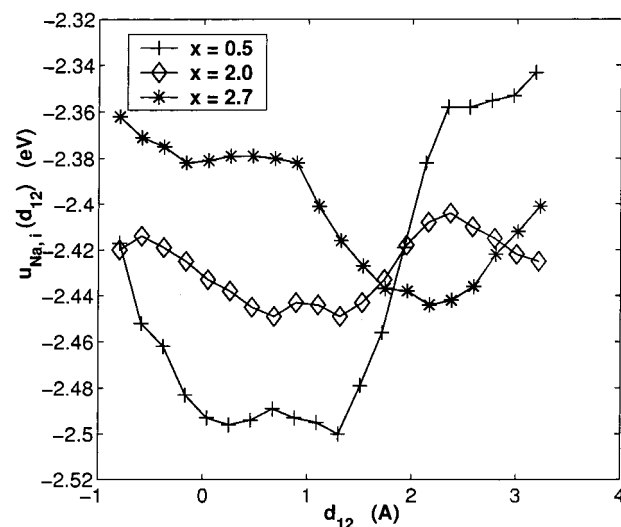


Figure 9. Potential energy profile as the Na⁺ ion hops from Na(1)–Na(2) through the mid-Na site, obtained from NVE-MD simulations at 600 K.

$x = 2.7$ are the two end members where nonzero conductivity of Na⁺ is observed in simulation, while $x = 2$ belongs to the high conducting range of compositions. It is seen that for the $x = 0.5$ the energies of Na(1) and mid-Na sites are lower (hence more favorable) while that of Na(2) is higher. For $x = 2$ the energies of Na(1), mid-Na, and Na(2) are comparable and the energy profile shows smaller energy barriers for hops between sites. For $x = 2.7$, again the profile shows larger variations and Na(1) appears to be higher in energy than Na(2). These findings suggest that ions mobility or conductivity is highest when the potential energy landscape has only moderate or low intensity undulations. This is the case with $x = 2$ which leads to lower activation energy and high mobility. These findings are identical to that found by Chitra and Yashonath³⁵ for diffusion of Lennard-Jones sorbates of different sizes within NaY zeolite: a rather flat potential energy landscape was found to be associated with high self-diffusivity. It may appear puzzling (see Figure 9) that for all the compositions the minimum energy is neither at Na(1) or Na(2) but somewhere between, suggesting the mid-Na site is more favored which is not consistent with the Na⁺ occupancies shown in Figure 5. This is because the appropriate quantity to be considered here is the free energy (ΔF) which will account for the entropy variations as well as the variations in energy, along the hop path. The entropy contributions are important as different sites have different Na–O distances (see Figure 4) and coordination numbers, which will influence the density of states of Na⁺ ions (or in a crude sense, the volume accessible by Na⁺ ions). The fact that the Na–O distances at the various sites depend on the composition emphasizes the role of entropy on the site occupancies as well as in deciding the free energy barrier for site to site hops.

The free energies have been calculated from the populations of Na⁺ ions, $P(d_{12})$, over the entire pathway connecting Na(1) and Na(2). Here d_{12} is treated as the diffusion coordinate akin to a reaction coordinate. The free energy ($\Delta F(d_{12})$) is calculated from^{25,36}

$$\Delta F(d_{12}) = -k_B T \ln(P(d_{12})) \quad (4)$$

where T is the temperature in Kelvin and k_B is the Boltzmann constant. The above expression is valid within the canonical ensemble. In the present simulation the sub system consisting of Na⁺ ions is in contact with the larger system consisting of

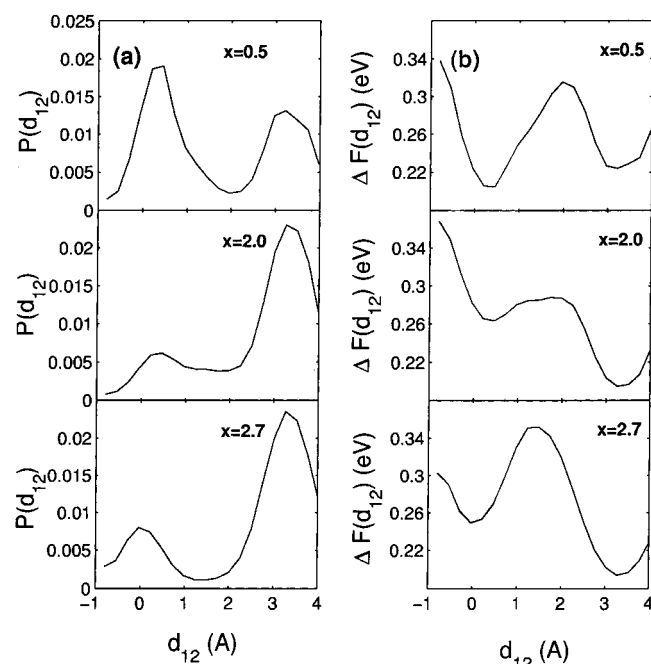


Figure 10. (a) The population of Na^+ , $P(d_{12})$, along its hop-path, $\text{Na}(1)$ –mid- Na – $\text{Na}(2)$, as a function of distance, d_{12} , of the Na^+ from $\text{Na}(1)$ and (b) the free energy ($\Delta F(d_{12})$) deduced from $P(d_{12})$ (eq 4).

the framework ions and therefore they essentially are in the canonical ensemble at constant temperature. The Na^+ population along the $\text{Na}(1)$ – $\text{Na}(2)$ path, $P(d_{12})$, and the corresponding free energy profiles, $\Delta F(d_{12})$, for three different compositions $x = 0.5$, 2, and 2.7, are shown in Figure 10a and 10b, respectively. It can be seen that for $x = 0.5$ the population of $\text{Na}(1)$ is larger than that of $\text{Na}(2)$ while for $x = 2.7$ the population in $\text{Na}(2)$ is higher than that in $\text{Na}(1)$. For the compositions with low conductance $x = 0.5$ and 2.7, the free energy barriers for the $\text{Na}(1)$ to $\text{Na}(2)$ hop is higher compared to that of the high conducting $x = 2$ composition.

It is seen in Figure 10b that there is no local minimum in the free-energy profile at $d_{12} = 1.7$ – 1.8 Å, that corresponds to the mid- Na position. In fact, the mid- Na region corresponds neither to a minimum nor a maximum but is rather flat. We see that at $x = 2$ there is considerable population (Na^+ of about 0.6) around this region and a somewhat lesser (Na^+ of 0.3) but nonzero population at $x = 0.5$ and 2.7. This suggests that mid- Na site is a rather spatially extended one (unlike the $\text{Na}(1)$ or $\text{Na}(2)$). Cherkaoui et al.³⁴ found in their NMR studies evidence for the presence of mid- Na site between $\text{Na}(1)$ and $\text{Na}(2)$. However, none of the X-ray diffraction studies prior to those by Boilot et al.²⁴ could identify this site probably because of the highly delocalized nature of this site. Neutron diffraction experiments on $\text{Na}_3\text{Zr}_2\text{Si}_2\text{PO}_{12}$ by Baur et al.¹² also failed to identify this site, even though they do observe a deficiency of around 0.6 Na^+ per unit formula. Note that the deficiency in their density matches well with the density of Na^+ ions at the mid- Na site obtained by us. The probability distribution function of Na^+ , deduced from their density along the $\text{Na}(1)$ – $\text{Na}(2)$ channel through X-ray diffraction studies, also does not show any features in support of the existence of the mid- Na site.¹¹ This is consistent with the contour diagram of Na^+ density shown in Figure 7 where no local maximum in density is seen between $\text{Na}(1)$ and $\text{Na}(2)$. The highly delocalized nature of the mid- Na site around $x = 2$ is likely to arise from the attempt of Na^+ ions to increase the mean separation among themselves suggesting a high degree of Na^+ – Na^+ correlation. This ion–ion

correlation appears to be one of the causes, among others, for the high Na^+ mobility near $x = 2$.

It is evident that the site occupancies (see Figure 5) are higher for the mid- Na site as compared to the $\text{Na}(1)$ site for intermediate compositions ($1.0 < x < 2.5$). From Figure 10b it is seen that in the intermediate composition, the free energy of $\text{Na}(1)$ site is almost comparable with those of mid- Na site. The fact that we do not shift the site positions with compositions gives rise to this apparent anomaly where the mid- Na site has a larger population than $\text{Na}(1)$. This, however, may be attributed to the inaccuracies in assigning Na^+ to a given site and the assumption that the site positions are unaltered with x .

It has been suggested by Kohler and Shulz that there are two bottlenecks, in the $\text{Na}(1)$ – $\text{Na}(2)$ hop path.¹¹ These bottlenecks are formed by triangular arrangement of oxygens, with their centers roughly at a distance of $1/3$ and $2/3$ of the $\text{Na}(1)$ – $\text{Na}(2)$ separation, from $\text{Na}(1)$. The first bottleneck, nearer to $\text{Na}(1)$, BN1, is formed by one triangular face of the $\text{Na}(1)\text{O}_6$. The other bottleneck, BN2, shares two oxygens (an edge of the $\text{Na}(1)\text{O}_6$) with BN1 while the third oxygen belongs to the $\text{Na}(2)\text{O}_8$. It may be noticed that the free energy profiles along the $\text{Na}(1)$ – $\text{Na}(2)$ hop path (Figure 10b) do not show any barriers (except the slight shoulder in the case of $x = 0.5$ at $d_{12} = 1.0$ Å) where the bottlenecks BN1 and BN2 are located. This is in contrast with the previous MD study,¹⁹ based on a rigid framework assumption, on rhombohedral $\text{LiZr}_2(\text{PO}_4)_3$ where the bottlenecks (BN1 and BN2) did give rise to barriers for hops, even for the smaller Li^+ ion. The reason for the disappearance of the barriers at BN1 and BN2 in $\text{Na}_{1+x}\text{Zr}_2\text{Si}_x\text{P}_{3-x}\text{O}_{12}$ could be static and dynamic changes of the framework from its ideally stacked polyhedra. Of the static changes in the framework, the predominant one in the present context is the anomalous expansion of the $\text{Na}(1)\text{O}_6$, shown in Figure 4. This expansion of $\text{Na}(1)\text{O}_6$ near $x = 2$ causes widening of bottlenecks (as the bottleneck, BN1, is formed entirely by the triangular face of the $\text{Na}(1)\text{O}_6$ as well as one edge of BN2) and could be thus offering a lower free energy barrier for the Na^+ hops for compositions near $x = 2$. A probable dynamic breathing-like motion of these bottleneck oxygens that is coupled with Na^+ hops may also be assisting the latter, along with the static widening of the bottlenecks discussed above. These are aspects that require further, more-detailed analysis of the NVE-MD trajectories.

Conclusions

The recently proposed interionic potential has been found to predict known quantities relating to structure, conductivity, and other properties in good agreement with experiments. In view of the good agreement, it appears reasonable to expect that the other properties that may be obtained with the help of this model will be reliable and correct. Many of the results are in excellent agreement with the X-ray diffraction results of Boilot et al.¹ For example, the sum of the sodium occupancy at the $\text{Na}(1)$ and mid- Na site add up to unity. The preferred conduction channel is found to be the one connecting $\text{Na}(1)$ and $\text{Na}(2)$ sites. Present study suggests that the anomalous behavior in the c parameter may arise from the anomalous behavior of $\text{Na}(1)$ – O distance. Variation in the a parameter probably arises from similar variation in the $\text{Na}(2)$ – O distance. Free energy profiles obtained point to the importance of entropy.

Additional work is required to clarify the role of framework and role of rotation of the polyhedra in giving the observed behavior of conductivity with composition x . Role of ion–ion repulsion in the resulting increase in conductivity and structural change also needs to be investigated.

Acknowledgment. The authors gratefully acknowledge support from Department of Science and Technology, New Delhi, under a project entitled *Investigations into Diffusion of Polyatomic Molecules through Porous Media*. We are thankful to Professor A. M. Umarji for useful discussions regarding Nasicon structure and properties and Professor K. J. Rao for kind encouragement.

References and Notes

- (1) Boilot, J. P.; Collin, G.; Colomban, Ph. *J. Solid State Chem.* **1988**, 73, 160.
- (2) Hong, H. Y-P. *Mater. Res. Bull.* **1976**, 11, 173.
- (3) Goodenough, J. B.; Hong, H. Y-P.; Kafalas, J. A. *Mater. Res. Bull.* **1976**, 11, 203.
- (4) Agrawal, D. K. *Trans. Ind. Ceram. Soc.* **1996**, 55, 1.
- (5) Alamo, J.; Roy, R. *Commun. Am. Ceram. Soc.* **1984**, 67, C-78.
- (6) Lenain, G. E.; McKinsty, H. A.; Limaye, S. Y.; Woodward, A. *Mater. Res. Bull.* **1984**, 19, 1451.
- (7) Oota, T.; Yamai, I. *J. Am. Ceram. Soc.* **1986**, 69, 1.
- (8) Yamamoto, K.; Abe, Y. *J. Am. Ceram. Soc.* **1998**, 81, 2201.
- (9) Boilot, J. P.; Salanié, J. P.; Desplanches, G.; Le Potier, D. *Mater. Res. Bull.* **1979**, 14, 1469.
- (10) von Alpen, U.; Bell, M. F.; Wichelhaus, W. *Mater. Res. Bull.* **1979**, 14, 1317.
- (11) Kohler, H.; Schulz, H. *Mater. Res. Bull.* **1985**, 20, 1461.
- (12) Baur, W. H.; Dygas, J. R.; Whitmore, D. H.; Faber, J. *Solid State Ionics* **1986**, 18 & 19, 935.
- (13) Kohler, H.; Schulz, H. *Mater. Res. Bull.* **1986**, 21, 23.
- (14) Tran Qui, D.; Capponi, J. J.; Joubert, J. C.; Shannon, R. D. *J. Solid State Chem.* **1981**, 39, 219.
- (15) Martinez-Juárez, A.; Pecharromán, C.; Iglesias, J. E.; Rojo, J. M. *J. Phys. Chem. B* **1998**, 102, 372.
- (16) Mazza, D. *J. Solid State Chem.* **2001**, 156, 154.
- (17) Vashishta, P.; Rahman, A. *Phys. Rev. Lett.* **1978**, 40, 1337.
- (18) Walker, J. R.; Catlow, C. R. A. *J. Phys. C: Solid State Phys.* **1982**, 15, 6151.
- (19) Padma Kumar, P.; Yashonath, S. *J. Phys. Chem. B* **2001**, 105, 6785.
- (20) Padma Kumar, P.; Yashonath, S. *J. Phys. Chem. B* **2002**, 106, 3443.
- (21) Colomban, Ph. *Solid State Ionics* **1986**, 21, 97.
- (22) Padma Kumar, P.; Yashonath, S. *J. Am. Chem. Soc.* **2002**, 124, 3828.
- (23) Huheey, J. E. *Inorganic Chemistry: Principles of Structure and Reactivity*, 3rd ed.; Harper & Row: Singapore, 1983.
- (24) Boilot, J. P.; Collin, G.; Colomban, Ph. *Mater. Res. Bull.* **1987**, 22, 669.
- (25) Frenkel, D.; Smith, B. *Understanding Molecular Simulation*; Academic Press: San Diego, 1996.
- (26) Allen, M. P.; Tildesley, D. J. *Computer Simulation of Liquids*; Clarendon: Oxford, 1996.
- (27) Nosé, S. *Mol. Phys.* **1984**, 52, 255.
- (28) Hazen, R. M.; Finger, L. W.; Agrawal, D. K.; McKinsty, H. A.; Perrotta, A. J. *J. Mater. Res.* **1987**, 2, 329.
- (29) Lenain, G. E.; McKinsty, H. A.; Alamo, J.; Agrawal, D. K. *J. Mater. Sci.* **1987**, 22, 17.
- (30) Alamo, J.; Roy, R. *J. Mater. Sci.* **1986**, 21, 444.
- (31) Chandler, D. *J. Phys. Chem.* **1978**, 68, 2959.
- (32) Montgomery, J. A.; Chandler, D.; Berne, B. J. *J. Phys. Chem.* **1979**, 70, 4056.
- (33) Kohler, H.; Schulz, H.; Melnikov, O. *Mater. Res. Bull.* **1983**, 18, 1143.
- (34) Cherkaoui, F.; Villeneuve, G.; Delmas, C.; Hagenmuller, P. *J. Solid State Chem.* **1986**, 65, 293.
- (35) Rajappa, C.; Yashonath, S. *J. Chem. Phys.* **1999**, 110, 5960.
- (36) Reif, F. *Fundamentals of Statistical and Thermal Physics*; McGraw-Hill: New York, 1985.